Supplementary Information

Engineering Covalent Organic Frameworks for Decoupled Photocatalytic and Dark Photocatalytic Synthesis of H_2O_2

Tian Wang[a], Du-Yong Chen[a], Xin-Feng Li[a], Hao Wang[a], Jing Li[a], Lu-Lu Hao[a], Yan Fang[1], Yu Shan[a], Liang Zhao[a], Shu-Xin Chen[d],Yingying Ning[d], Yin-Shan Meng*[a, c], Jiyun Hu*[b], and Tao Liu*[a, c]

[a] State Key Laboratory of Fine Chemicals, Frontier Science Center for Smart Materials, School of Chemical Engineering, Dalian University of Technology, No.2 Linggong Road, Dalian 116024, China; Liaoning Binhai Laboratory, Dalian 116023, China.

[b] Dongguan Key Laboratory of Interdisciplinary Science for Advanced Materials and Large-Scale Scientific Facilities, School of Physical Sciences, Great Bay University, Dongguan 523000, China.

[c] Liaoning Binhai Laboratory, Dalian 116023, China.

[d] Spin-X Institute, School of Chemistry and Chemical Engineering, School of Biomedical Sciences and Engineering, State Key Laboratory of Luminescent Materials and Devices, Guangdong-Hong Kong-Macao Joint Laboratory of Optoelectronic and Magnetic Functional Materials, South China University of Technology, Guangzhou 510641, China.

*Corresponding Author(s): Tao Liu: liutao@dlut.edu.cn; Jiyun Hu: hujiyun@gbu.edu.cn; Yin-Shan Meng: mengys@dlut.edu.cn

1 General Considerations

1.1 Instruments

Powder X-ray diffraction (PXRD) patterns were collected on a SmartLab 9KW desktop X-Ray diffractometer operated at 30 kV and 15 mA (step = 0.01°, scan rate = 2 °/min). FT-IR spectra were recorded using a PerkinElmer Spotlight 400 FT-IR spectrometer and a ThermoFisher Nicolet 6700 FT-IR spectrometer equipped with an attenuated total reflectance (ATR) accessory. Liquid NMR experiments were carried out on a Bruker AVANCE III 500 and a Bruker Avance II 400. Solid State NMR experiments were carried out on an Agilent DD2-500MHz (14.25 T) DD2 spectrometer equipped with a 3.2 mm HCN Balun probe with samples spinning at 10 kHz. X-ray photoelectron spectroscopy (XPS) studies were performed with an ESCALAB Xi+ XPS instrument. Scanning Electron Microscopy (SEM) images were recorded with a Hitachi SU88220 scanning electron microscope. The UV-VIS spectra and diffuse reflectance spectra were collected with a Hitachi UH4150. Thermogravimetric analysis (TGA) measurements were performed on a TA Q600 instrument. The samples were heated from room temperature to 800 °C under N_2 flow (25 ml min^{-1}) at a heating rate of 10 K min^{-1}. Steady-state photoluminescence (PL) and time-resolved PL spectra were obtained on the Steady State Transient Fluorescence Spectrometer FLS-1000. N_2 sorption isotherms were obtained on an Autosorb-IQ-MP/XR Automated Gas Sorption Analyzer at 77 K. All the samples were vacuum activated at 120 °C overnight on the instrument before analysis. Electron paramagnetic resonance (EPR) measurements were recorded on the Bruker E500 instrument at the X-band frequency (9.4 GHz). Crystal models were generated using Materials Studio version 7.0 software.

1.2 Computational detail

DFT calculations were conducted using the CP2K package based on a hybrid Gaussian and plane-wave (GPW) method with Goedecker-Teter-Hutter (GTH) pseudopotentials.[1-3] The generalized gradient approximation with the Perdew-Burke-Ernzerhof (PBE) functional was employed to describe the exchange-correlation interactions [4]. A plane-wave energy cutoff of 500 Ry was adopted, and the Brillouin zone sampling was performed using a 1 × 1 × 3 Monkhorst-Pack k-point mesh for surface calculations. Geometry optimizations were conducted until the convergence criteria were met, specifically with a maximum step size of less than 0.003 Å and a root-mean-square (RMS) step size below 0.0015 Å. The van der Waals (vdW) interactions were corrected by applying Grimme's dispersion correction method (DFT-D3) with zero damping[5].

Gibbs free energies were calculated as $\Delta G = \Delta E + \Delta E_{ZPE} - T\Delta S$, where ΔE, ΔE_{ZPE}, and ΔS represent the differences in electronic energy, zero-point energy, and entropy between the products and reactants, respectively. Zero-point energies for intermediates in both isolated and adsorbed states were calculated by vibrational frequency analysis, while the vibrational frequencies and entropy values of gas-phase species were obtained from the National Institute of Standards and Technology (NIST) database.[6, 7]

The TDDFT calculations were performed using the CP2K program[3], To describe the electronic structure, we employed plane waves with a cutoff of 400 Ry and a Gaussian basis set: 6-31G** for all elements. The exchange-correlation potential is described by using the generalized gradient approximation of Perdew-Burke-Ernzerhof (GGA-PBE). Although the PBE functional will underestimate the excitation energy and band gap, this calculation study mainly focuses on the migration of electrons and does not require precise values of the excitation energy and band gap. We use the electron-hole analysis method[8] to examine the transfer of electrons after they are excited. Data processing was conducted using Multiwfn software[9].

1.3 Materials and Reagents.

All materials were purchased from Innochem and used without further purification.

1.4 Electrochemical measurement

Electrochemical measurements were conducted with the Chi760e electrochemical workstation from Chenhua Instrument. A traditional three-electrode system was used with a COF-based working electrode, platinum wire as the counter electrode, and Ag/AgCl (saturated KCl) as the reference electrode. The electrolyte was a 0.5 M Na_2SO_4 aqueous solution. 4 mg COF powder was mixed with 50 μL of Nafion and 250 μL of ethanol, ultrasonicated for 30 min to obtain a slurry. The suspension was spread onto the surface of the glassy carbon electrode (d=3 mm), forming a film after air drying. Then, the photocurrent response was measured under illumination from a 300 W Xe lamp (Beijing Perfect S4 light, PLS-SXE300/300UV) at an applied bias of 0.4 V. Electrochemical impedance spectroscopy (EIS) curves were recorded at 10^{-2} to 10^{6} Hz.

1.5 Photocatalytic H_2O_2 production

Photocatalytic H_2O_2 production: 4 mg of photocatalyst was dispersed in 50 mL of water. The suspension was allowed to stand in the dark for 30 minutes. A 300 W Xe lamp (CEL-HXF300, China) with full-spectrum was used as the light source during the measurement. The concentration of H_2O_2 was determined by a UV-vis spectrophotometer. 2 mL of liquid was filtered with a 0.22 μm filter to remove the COFs. The sample was mixed with pre-prepared $Ce(SO_4)_2$ solution, and the concentration of H_2O_2 was determined by the UV-vis spectroscopy (Eq. S1).

$$2Ce^{4+} + H_2O_2 \longrightarrow 2Ce^{3+} + 2H^+ + O_2 \text{ (Eq. S1)}$$

The concentration of produced H_2O_2 can be calculated by Eq. S2:

$$c_{H_2O_2} = \frac{1}{2} \triangle c_{Ce^{4+}} \text{ (Eq. S2)}$$

By adding a known concentration of H_2O_2 solution into the $Ce(SO_4)_2$ solution, the change of absorption intensity at about 316 nm was measured with the UV-vis spectrometer. The linear relationship between Ce^{4+} concentration and the absorption intensity was established as follows：

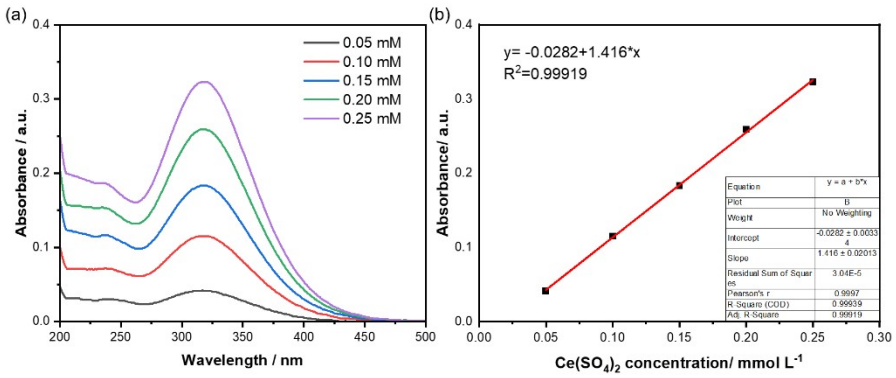

The equation for calculating the quantity of H_2O_2,

$$n_{H_2O_2}(\text{mol g}^{-1}) = \frac{V \times c_{H_2O_2}}{2m_{COF}}$$

$$r_{H_2O_2}(\text{mol g}^{-1}\text{h}^{-1}) = \frac{n_{H_2O_2}(\text{mol g}^{-1})}{t}$$

$$Q_{per\ g}(\text{C g}^{-1}) = zFn_{H_2O_2}(\text{mol g}^{-1}) = 2Fn_{H_2O_2}(\text{mol g}^{-1})$$

$$F \approx 96485 \text{ C mol}^{-1}$$

where $c_{H_2O_2}$ is the concentration of hydrogen peroxide in the solution after photocatalysis, m_{COF} is the mass of the COF (4 mg) used in the photocatalytic reaction, $n_{H_2O_2}$ is the molar amount of hydrogen peroxide produced during the photocatalytic process, $r_{H_2O_2}$ is the rate of hydrogen peroxide formation, $Q_{per\ g}$ represents the quantity of stored electrons per gram of COF as determined from the amount of hydrogen peroxide generated under dark conditions, and F is the Faraday constant (96485 C mol^{-1}).

2 Synthesis and characterization of COFs

2.1 Synthesis of monomers

Synthesis of 1,3,6,8-tetrakis(4-aminophenyl)pyrene (TAPPy)

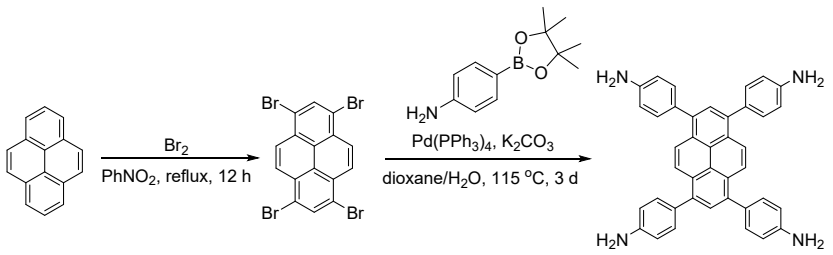

1,3,6,8-tetrabromopyrene. Pyrene (5.00 g, 0.0247 mol) and Br_2 (7 mL) were heated in 100 mL of nitrobenzene at 120 °C overnight. After cooling to room temperature, the pale-green precipitate was filtered, washed with ethanol, and dried.

1,3,6,8-tetrakis(4-aminophenyl)pyrene. 1,3,6,8-tetrabromopyrene (1.48 g, 2.9 mmol), 4-aminophenylboronic acid pinacol ester (3.01 g, 13.7 mmol), K_2CO_3 (2.18 g, 15.7 mmol), and $Pd(PPh_3)_4$ (330 mg, 0.3 mmol, 10 mol%) were mixed in 32 mL 1,4-dioxane and 8 mL H_2O in a 150 mL thick-wall pressure bottle and bubbled with argon gas for 20 min. The tube was then capped and heated at 115 °C in an oil bath for three days. After cooling to room temperature, a yellow solid was precipitated by adding water. After filtration, the yellow solid was rinsed three times with methanol and finally dried overnight in a vacuum oven. Yield: 1.76 g, 85%. ^{1}H NMR (400 MHz, DMSO-d_6): 8.13 (s, 4 H), 7.79 (s, 2 H), 7.34 (d, J = 8.4 Hz, 8 H), 6.77 (d, J = 8.5 Hz, 8 H), 5.30 (s, 8 H).

2.2 Synthesis of COFs

Synthesis of Py-1P COF.[10] Compound **1** (40.5 mg, 0.0715 mmol), 1,4-Phthalaldehyde (19.2 mg, 0.143 mmol), and 1,4-dioxane/mesitylene (1 mL, 4/1) were added to a 10 mL vial. The mixture was sonicated thoroughly (1-2 minutes). The vial was preheated to 70 °C using an aluminum heating block. To the preheated solution, 0.5 mL of 10.5 M acetic acid was added. The vial was capped securely and gently swirled to mix the acid into the reaction mixture. The mixture was then maintained at 70 °C for 4 hours. Afterwards, the COF solid was filtered off and rinsed thoroughly with THF, acetone, and hexane. The powder was dried under vacuum at 60 °C. Yield: 52 mg.

Synthesis of Py-1Q COF.[11] Styrene oxide (45 mg, 0.375 mmol, 1.5 equiv), $Cu(OTf)_2$ (27 mg, 0.074 mmol, 0.3 equiv.), and Py-1P COF (52 mg, imine 0.25 mmol) were dissolved in 1 mL of DMSO in a 5 mL flask. The reaction was capped with a septum and heated under oxygen to 80 °C for 3

days. The precipitate was collected via filtration, and Soxhlet extracted with THF, acetone, and methanol in turn. The powder was dried at 120 °C under vacuum to give orange Py-1Q COF in an isolated yield of 88%.

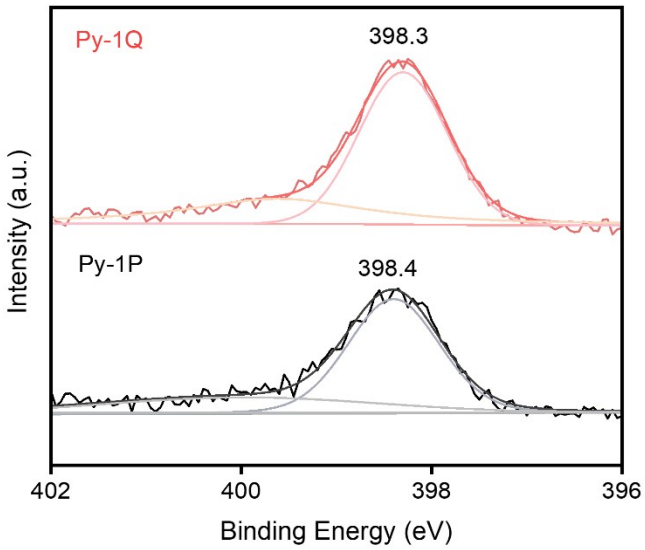

Fig S1. N 1s XPS spectra of Py-1P and Py-1Q COF.

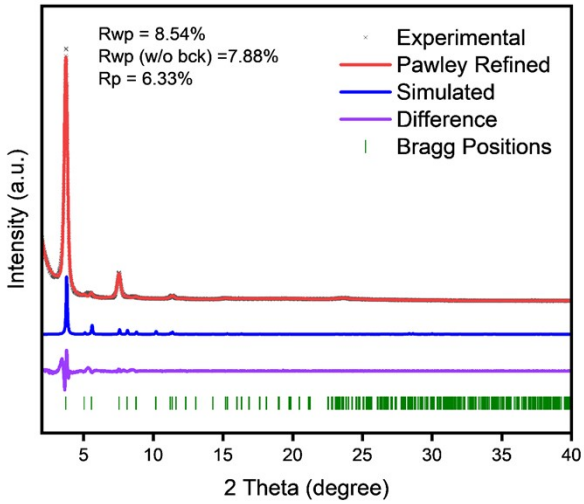

Fig S2. Experimental PXRD pattern (black dots) of Py-1Q COF. Pawley refinement (red line), Simulated PXRD pattern (blue line), difference plot between the experimental data and the Rietveld-refined PXRD pattern (purple line), and Bragg positions are indicated by green ticks.

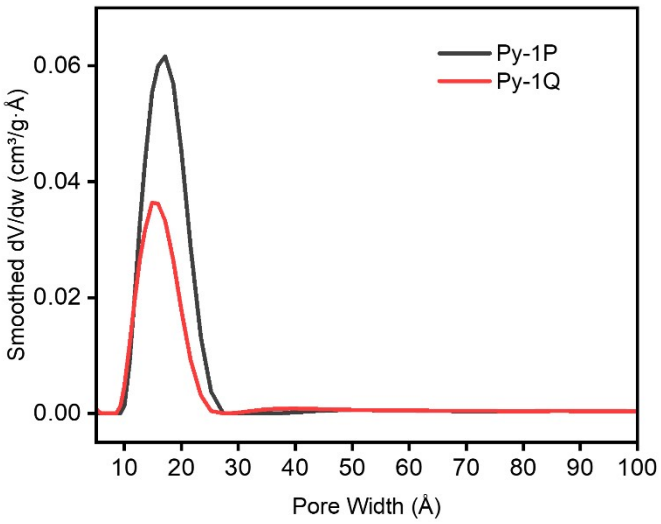

Fig S3. Pore size distribution profiles of Py-1P and Py-1Q COF.

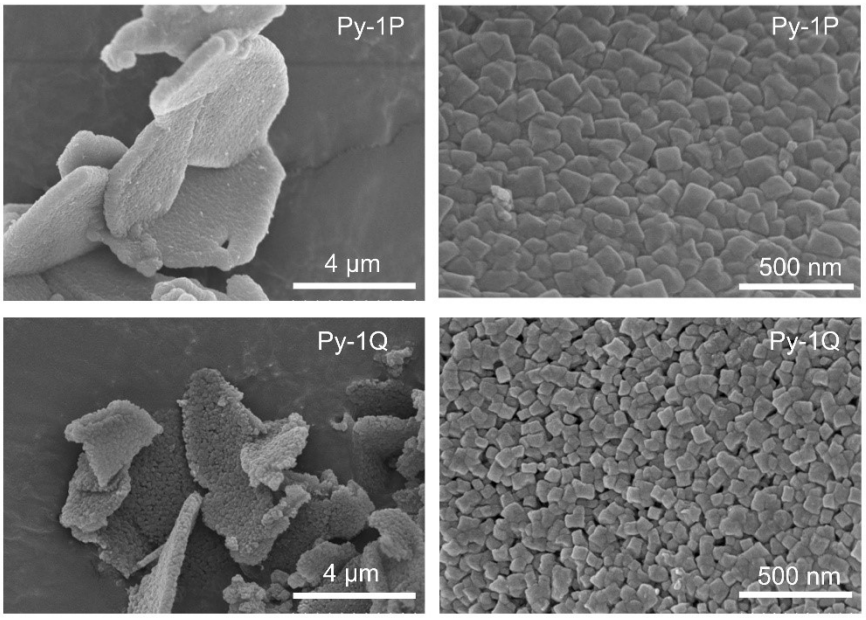

Fig S4. SEM images of Py-1P and Py-1Q COF.

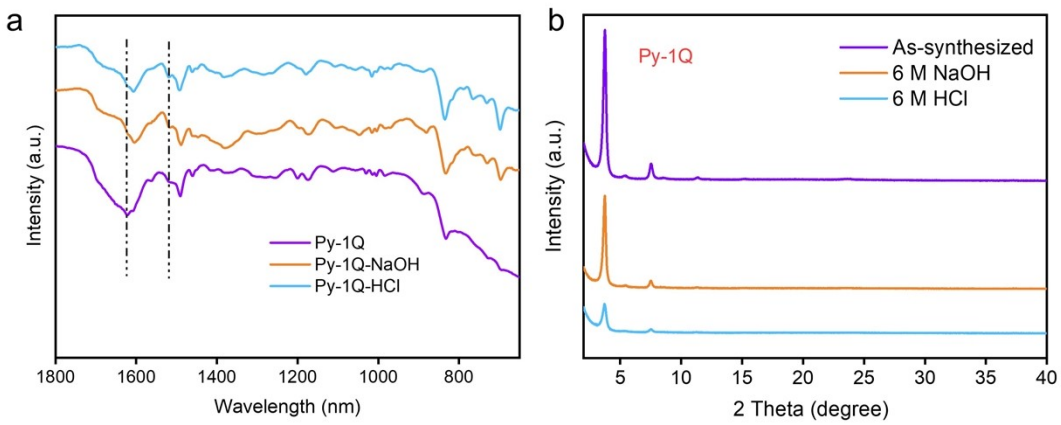

Fig S5. (a) FT-IR and (b) PXRD patterns of Py-1Q COF after treatment with various solvents for seven days.

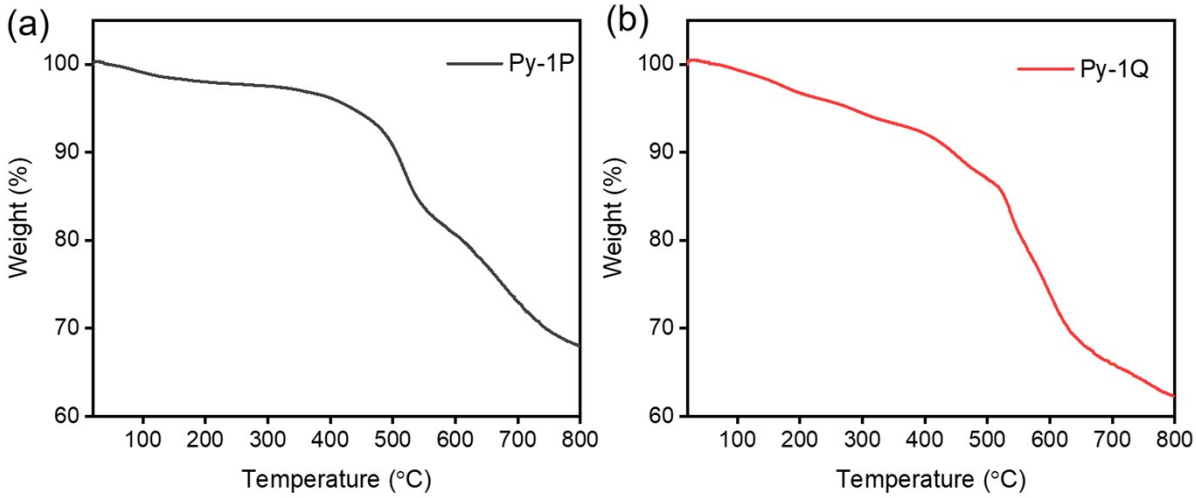

Fig S6. TGA trace of Py-1P and Py-1Q COF under N_2 from 25 to 800 °C.

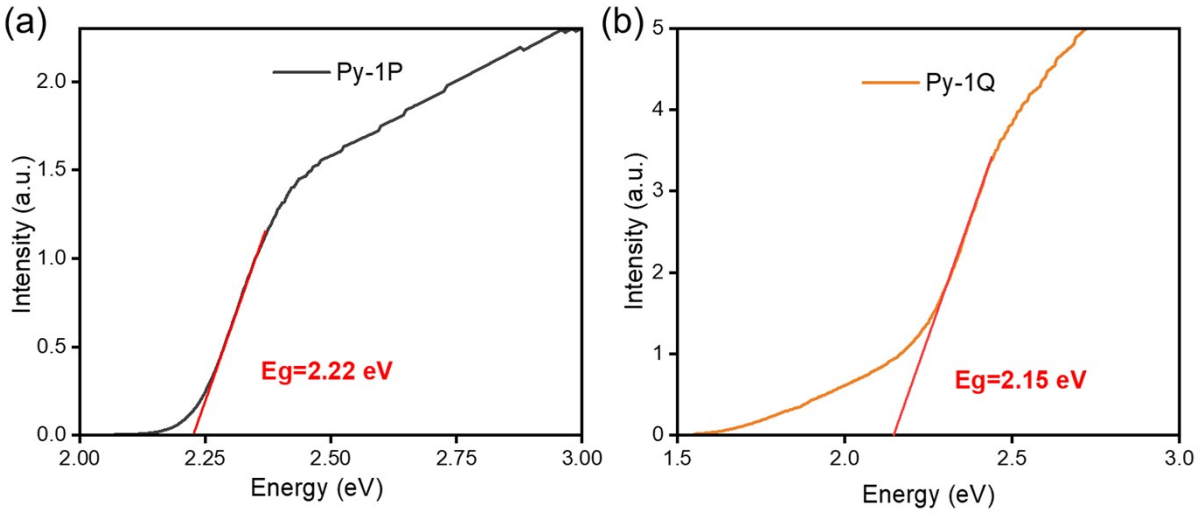

Fig S7. Tauc plots of Py-1P and Py-1Q COF.

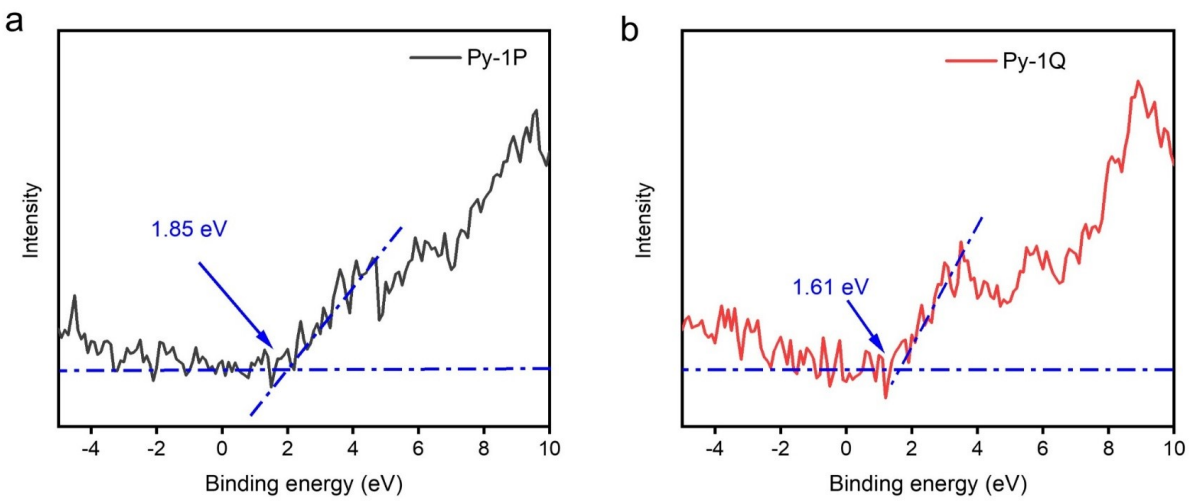

Fig S8. VB-XPS spectra of Py-1P and Py-1Q COF.

Calculation of Valence band energy (E_{VB}) and conduction band energy (E_{CB})

$$E_{VB\ (vs.\ vac)} = -\ (\phi + VB_{xps})$$

$$E_{VB\ (vs.\ NHE)} = -(4.44+E_{VB\ (vs.\ vac)})$$

$$E_{CB} = E_{VB} + E_g$$

E_g is the band gap derived from the UV-vis spectra, ϕ is the electron work function of the analyser (4.35 eV) and VB_{xps} is derived from valence band XPS spectra.

	$E_{VB\ (vs.\ vac)}$	$E_{VB\ (vs.\ NHE)}$	$E_{CB\ (vs.\ NHE)}$
Py-1P	-6.2	1.76	-0.46
Py-1Q	-5.96	1.52	-0.58

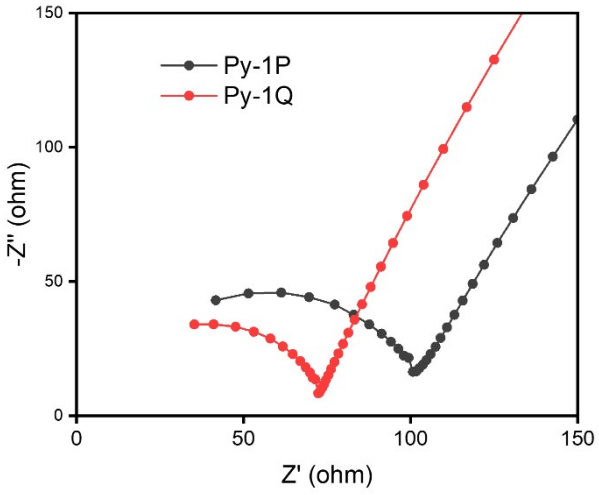

Fig S9. Nyquist plots of electrochemical impedance spectroscopy of Py-1P and Py-1Q COF.

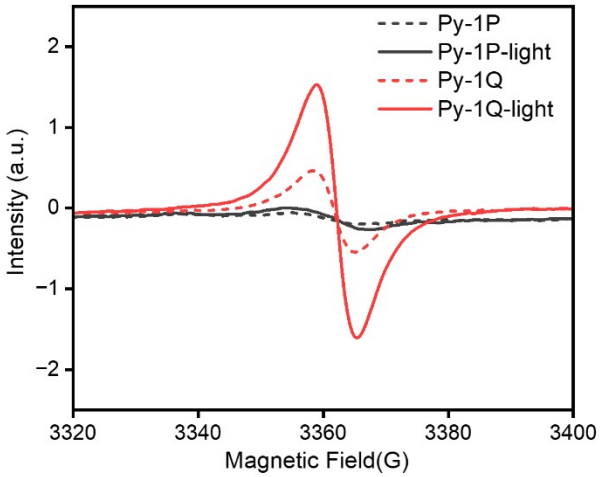

Fig S10. Solid state electron paramagnetic resonance (EPR) measurement of Py-1P and Py-1Q COF powders.

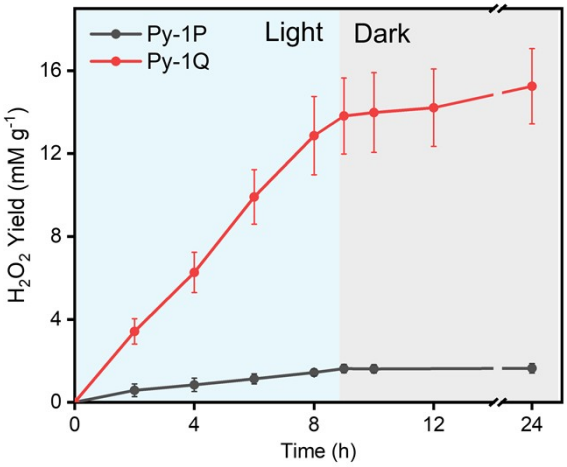

Fig S11. Error bars represent standard deviations from three independent catalytic experiments performed on Py-1Q and Py-1P.

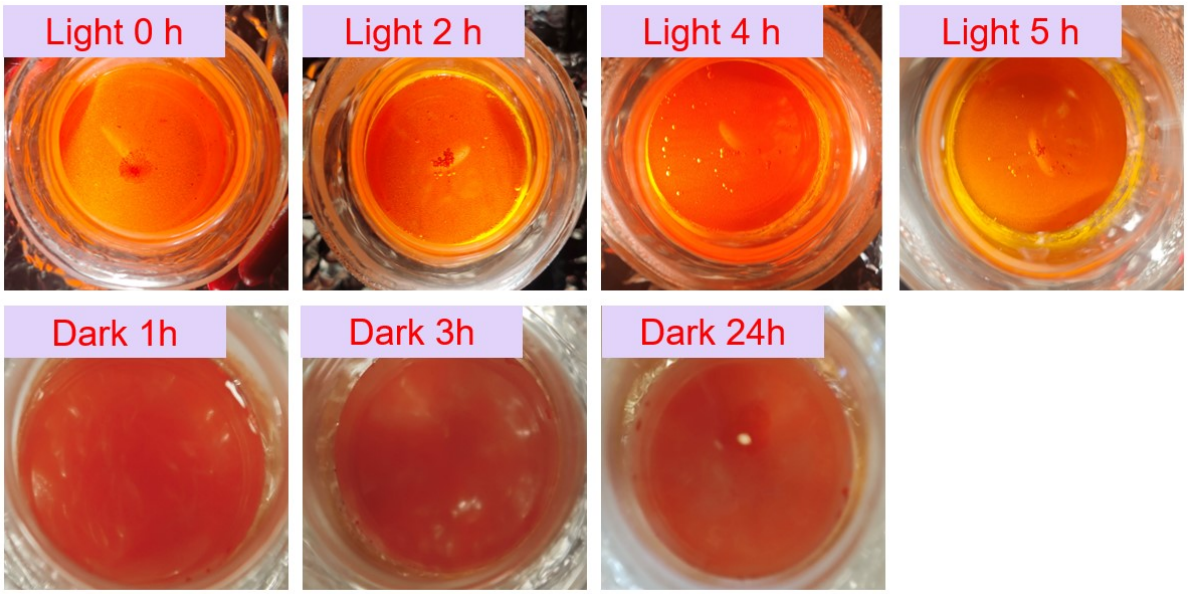

Fig S12. Color change of Py-1P COF during catalysis.

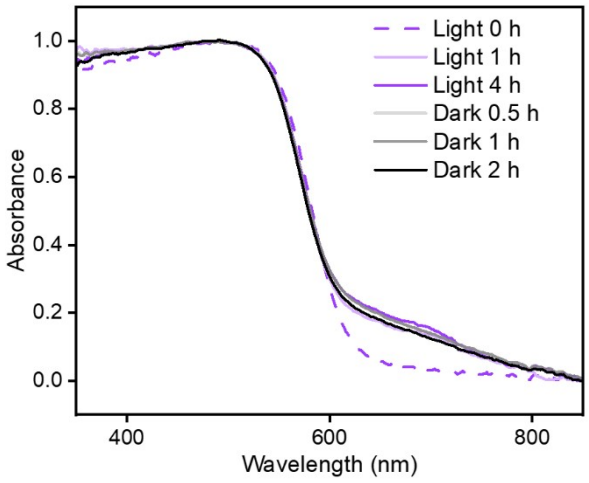

Fig S13. The DRS UV-Vis spectra of Py-1P COF under light irradiation and dark conditions (COF was dispersed in water and irradiated using a Xe lamp. Samples collected at different exposure intervals were transferred into 1 mm quartz cuvettes and analysed in reflectance mode).

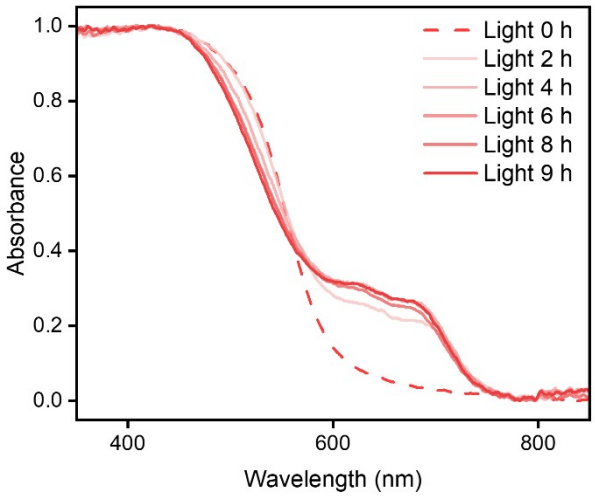

Fig S14. The DRS UV-Vis spectra of Py-1Q COF under light irradiation (COF was dispersed in water and irradiated using a Xe lamp. Samples collected at different exposure intervals were transferred into 1 mm quartz cuvettes and analyzed in reflectance mode).

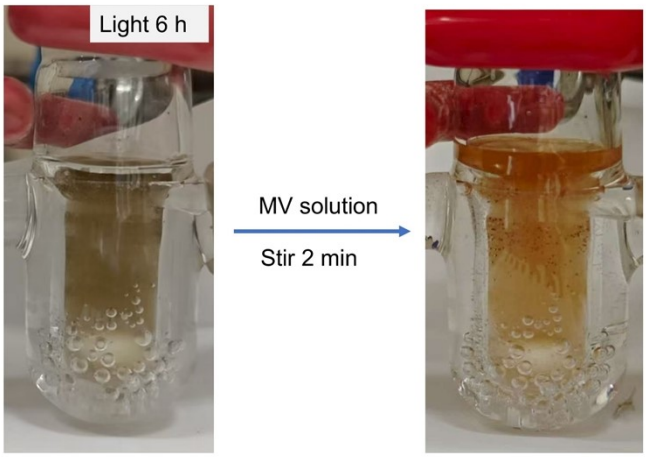

Fig S15. The images of Py-1Q COF under light irradiation for 6 h, and after adding the MV solution.

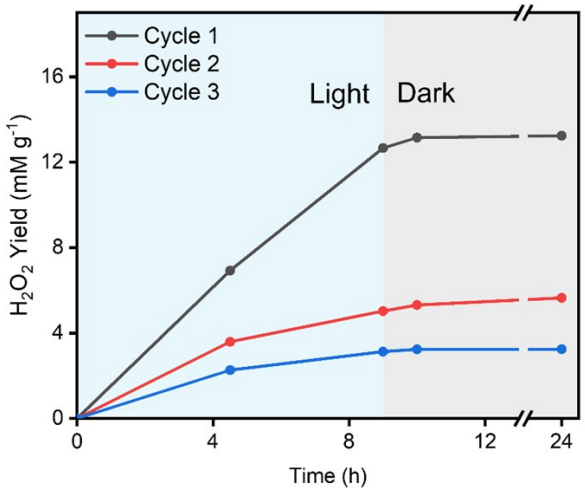

Fig S16. Cycling experiment of Py-1Q catalysis.

Fig S17. Photo and dark catalytic experiments of Py-1Q in the presence of 1 mg $Cu(OTf)_2$.

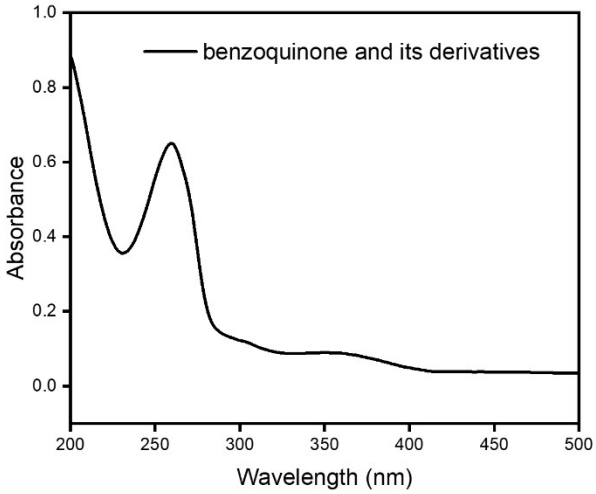

Fig S18. The UV-vis absorption spectrum of the reaction aliquot when p-benzoquinone was used as $O_2^{\bullet-}$ scavenger. (The reaction suspension turned black after the introduction of p-benzoquinone. The new unidentified absorption band at ca. 250 nm strongly interferes with the absorption band at 350 nm used for the H_2O_2 quantification.)

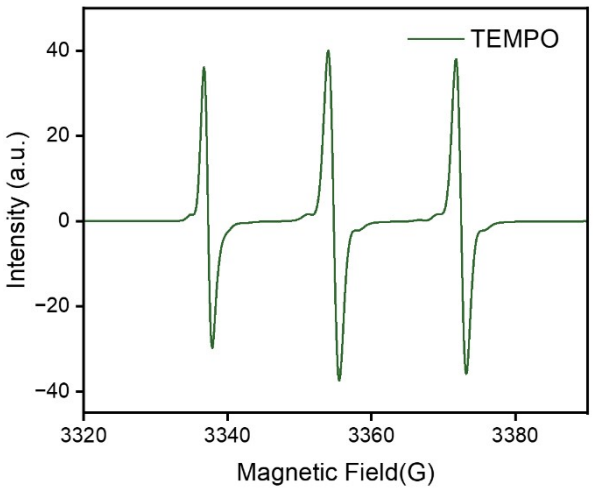

Fig S19. EPR spectra of 0.1 mM TEMPO in H_2O.

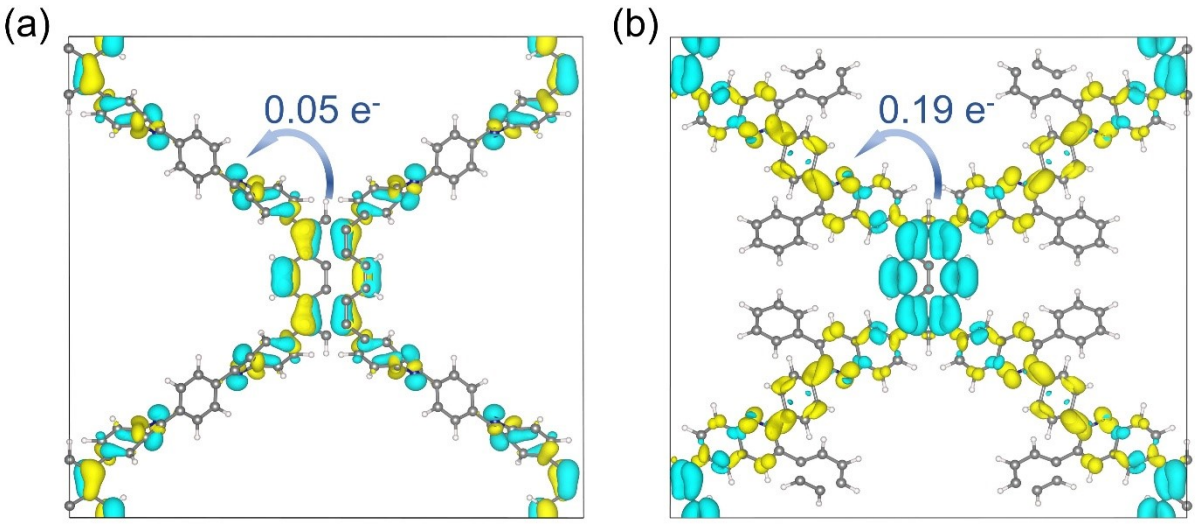

Fig S20. Excited-state electron transfer potential surface and calculated charge-transfer quantification of Py-1P and Py-1Q.

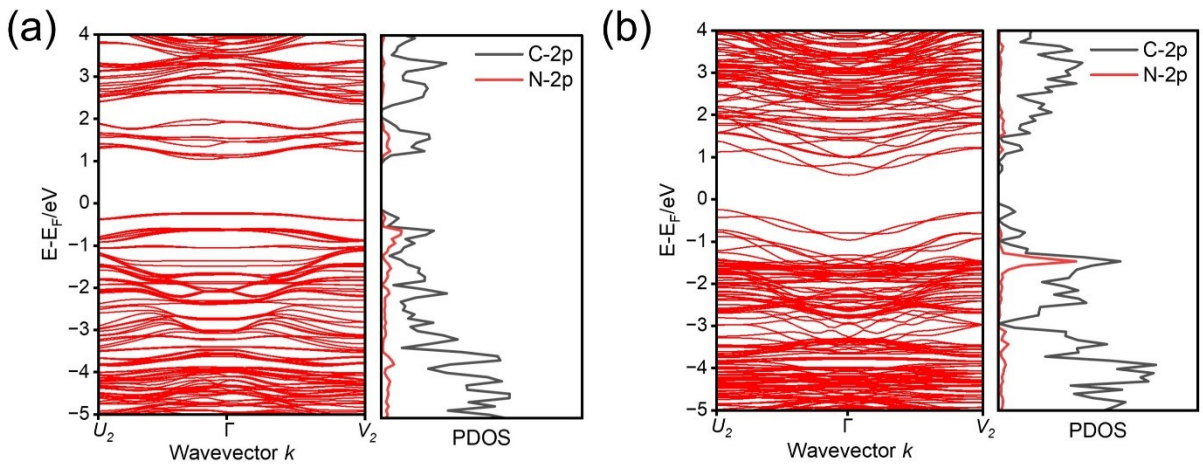

Fig S21. The band structure and PDOS of (a) Py-1P and (b) Py-1Q.

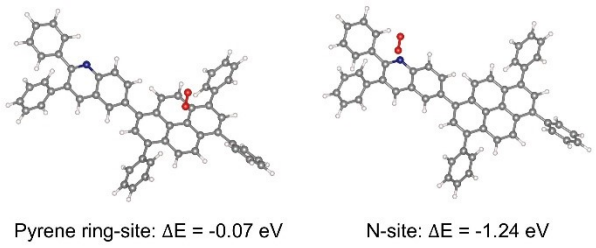

Fig S22. Calculated O_2 adsorption energy at Py-1Q.

Table S1. Comparison of H_2O_2 production performance for different COF photocatalysts reported in the literature.

Catalyst	Reaction condition	Light source	H_2O_2 rate (mmol g^{-1} h^{-1})	Reaction pathway	Ref.
Py-1P	**H_2O**	**Xe lamp**	**0.18**	**ORR、WOR**	**This work**
Py-1Q	**H_2O**	**Xe lamp**	**1.53**	**ORR、WOR**	**This work**
COF-BCTB-BT	H_2O (O_2-saturated)	Xe lamp	33.2	ORR	12
CTF-FL	H_2O	λ > 420 nm	2.412	ORR、WOR	13
CTF-BP	H_2O	λ > 420 nm	0.426	ORR	13
Imine-1	H_2O	λ > 420 nm	1.617	ORR	14
DMCR-1NH	H_2O	λ > 420 nm	2.264	ORR	14
DMCR-1	H_2O	λ > 420 nm	1.876	ORR	14
A-COF	H_2O	λ > 400 nm	1.16	ORR	15
H-COF	H_2O	λ > 400 nm	0.4	ORR	15
I-COF	H_2O	λ > 400 nm	0.304	ORR	15
CityU-41	H_2O (O_2-saturated)	Xe lamp	0.682	ORR、WOR	16
TAH-COF	H_2O	λ > 400 nm	6.003	ORR、WOR	17
TPPA-COF	H_2O	λ > 400 nm	0.905	ORR、WOR	17
BAH-COF	H_2O	λ > 400 nm	1.297	ORR、WOR	17
Py-Py-COF	H_2O: BA = 9:1	λ > 420 nm	1.242	ORR	18
COF-TfpBpy	H_2O	λ > 420 nm	0.694	ORR、WOR	19
HEP-TAPB-COF	H_2O (O_2-saturated)	λ > 420 nm	0.99	ORR、WOR	20
SonoCOF-F2	H_2O	λ > 420 nm	1.244	ORR	21
TB-COF	H_2O	400 nm≤ λ ≤ 700nm	5.186	ORR、WOR	22
TA-COF	H_2O	400 nm≤ λ ≤ 700nm	2.387	ORR、WOR	22
H_2Pc-THHI-COF	H_2O (O_2-saturated)	λ > 420 nm	4.511	ORR、WOR	23
TMT-TT-COF	H_2O	400 nm≤ λ ≤ 700nm	1.952	ORR	24
Thz-COF	H_2O (O_2-saturated)	λ > 420 nm	160	ORR、WOR	25
Imi-COF	H_2O (O_2-saturated)	λ > 420 nm	70	ORR、WOR	25
OH-COF	H_2O	λ > 420 nm	1.99	ORR	26
PTCOF	H_2O	λ > 420 nm	6.07	ORR、WOR	27
APT-BT COF	H_2O (O_2-saturated)	415 nm	2.47	ORR	28
BTT-AQ	H_2O	λ > 400 nm	4.2	ORR、WOR	29
TAPT-1KtTb Pd COF	H_2O	λ > 400 nm	8.56	ORR、WOR	30

ORR: oxygen reduction reaction; WOR: water oxidation reaction.

Table S2. Comparison of the electron storage capacity of different materials.

Materials	Category	Electron storage mechanism	Applications	Electron storage capacity (C g^{-1})[a]	Ref.
Py-1Q	**COF**	**radical**	**H_2O_2 production**	**277**	**This work**
CN-500–4	carbon nitride	radical	H_2 production	58.536	31
HPHI4	carbon nitride	radical	H_2O_2 production	37.98	32
ionic-CN/Co_3O_4	carbon nitride	radical	H_2 production	52	33
NCN-CN_x	carbon nitride	radical	H_2 production	34.16	34
Mel-PHI	carbon nitride	radical	H_2 production	5.81	35
MIL-125	MOF	Ti^{4+}/Ti^{3+} redox couple	H_2 production	33.7	36
ReCl-253	MOF	radical anion $[ReCl(CO)_3(5,5'\text{-}dcbpy)]^{\bullet-}$	H_2 production	14 (14.1)	37
MnBr-253	MOF	radical anion $[MnBr(CO)_3(dcbpy)]^{\bullet-}$	H_2 production	42	38
MIP-177(Ti)-LT	MOF	Ti^{4+}/Ti^{3+} redox couple	H_2 production	58	39
AgBiO-1	metal oxides	Ag^+/Ag redox couple	organic pollutant degradation	4.348	40
BiO-OVs	metal oxides	Ag^+/Ag redox couple	organic pollutant degradation	2.406	40
$NbWO_6$	metal oxides	polaron–cation complex	H_2 production	0.69	41

[a] The electron storage capacity was derived from the amount of the chemical product (value in parathesis was obtained from titration experiment with methylviologen).

Table S3. Unit cell parameters and fraction atomic coordinates for Py-1Q COF.

	C2/M (C2H-3)						
Calculated unit cell	a= 3.8381 Å, b= 31.0490 Å, c=35.0870 Å, α = γ = 90°, β = 95.334						
Atom	x	y	z	Atom	x	y	z
C1	0.83137	0.62666	0.43202	H20	0.45762	0.77714	0.31249
C2	0.8818	0.5487	0.46899	C21	0.2522	0.70379	0.23997
N3	0.52387	0.70243	0.33943	H22	0.24612	0.66606	0.23104
C4	0.71283	0.52371	0.44496	C23	0.89787	1.11532	1.25159
H5	0.57148	0.5424	0.42486	C24	1.09159	1.0767	1.25021
C6	0.90617	0.60007	0.46619	C25	1.10672	1.0555	1.28916
C7	0.85714	0.60866	0.38945	C26	0.92621	1.07211	1.32999
H8	0.97352	0.57384	0.37963	C27	0.72652	1.11023	1.33124
C9	0.63339	0.67822	0.36849	C28	0.71314	1.13148	1.29241
C10	0.72637	0.67278	0.43954	H29	0.80602	0.5775	0.31073
H11	0.71653	0.69001	0.47216	H30	1.23733	1.06255	1.21715
C12	0.74034	0.63335	0.35899	H31	1.26727	1.02436	1.28785
C13	0.72217	0.61416	0.31941	H32	0.94268	1.05475	1.3615
C14	0.63372	0.69806	0.40809	H33	0.57435	1.12395	1.36413
H15	0.55772	0.73529	0.41497	H34	0.55052	1.16237	1.29366
C16	0.37688	0.71697	0.2744	C35	1	0.52453	0.5
C17	0.50085	0.6858	0.30031	C36	1	0.62252	0.5
C18	0.60133	0.63924	0.28955	H37	1	0.6589	0.5
C19	0.36689	0.76422	0.28419				

REFERENCES

1. G. Kresse and D. Joubert, Physical Review B, 1999, 59, 1758-1775.
2. P. E. Blöchl, 1994, 50, 17953-17979.
3. J. Hutter, M. Iannuzzi, F. Schiffmann and J. VandeVondele, WIREs Computational Molecular Science, 2013, 4, 15-25.
4. K. Perdew Jp Fau - Burke, M. Burke K Fau - Ernzerhof and M. Ernzerhof, 1996, 77, 3865-3868.
5. S. Grimme, S. Ehrlich and L. Goerigk, J. Comput. Chem., 2011, 32, 1456-1465.
6. J. K. Nørskov, J. Rossmeisl, A. Logadottir, L. Lindqvist, J. R. Kitchin, T. Bligaard and H. Jónsson, J. Phys. Chem. B, 2004, 108, 17886-17892.
7. N. J. K. B. L. A. K. J. R. C. J. G. P. S. StimmingU., J. Electrochem. Soc., 2005, 152, J23-J26
8. Z. Liu, T. Lu and Q. Chen, Carbon, 2020, 165, 468-475.
9. T. Lu and F. Chen, J. Comput. Chem., 2011, 33, 580-592.
10. F. Auras, L. Ascherl, A. H. Hakimioun, J. T. Margraf, F. C. Hanusch, S. Reuter, D. Bessinger, M. Döblinger, C. Hettstedt, K. Karaghiosoff, S. Herbert, P. Knochel, T. Clark and T. Bein, J. Am. Chem. Soc., 2016, 138, 16703-16710.
11. S. Ali and A. T. Khan, Org. Biomol. Chem., 2021, 19, 3255-3262.
12. A. Kong, T. Yang, H. Yan, X. Chen, Y. Chen, F. Kang, Q. Zhang and R. Liu, J. Am. Chem. Soc., 2025, 147, 20855-20864.
13. L. Zhang, C. Wang, Q. Jiang, P. Lyu and Y. Xu, J. Am. Chem. Soc., 2024, 146, 29943-29954.
14. P. Das, G. Chakraborty, J. Roeser, S. Vogl, J. Rabeah and A. Thomas, J. Am. Chem. Soc., 2023, 145, 2975-2984.
15. S. Yang, D. Si, L. Zou, M. Shi, Y. Huang and R. Cao, J. Am. Chem. Soc., 2025, 147, 30287-30295.
16. L. Zhang, Z. Chen, X.-X. Li, X. Wang, Q. Gu, Z. Zheng, N. Aratani, C.-S. Lee, Y.-Q. Lan and Q. Zhang, J. Am. Chem. Soc., 2025, 147, 27847-27854.
17. T. Xu, Z. Wang, W. Zhang, S. An, L. Wei, S. Guo, Y. Huang, S. Jiang, M. Zhu, Y.-B. Zhang and W.-H. Zhu, J. Am. Chem. Soc., 2024, 146, 20107-20115.
18. J. Sun, H. Sekhar Jena, C. Krishnaraj, K. Singh Rawat, S. Abednatanzi, J. Chakraborty, A. Laemont, W. Liu, H. Chen, Y. Y. Liu, K. Leus, H. Vrielinck, V. Van Speybroeck and P. Van Der Voort, Angew. Chem. Int. Ed., 2023, 62, e202216719.
19. M. Kou, Y. Wang, Y. Xu, L. Ye, Y. Huang, B. Jia, H. Li, J. Ren, Y. Deng, J. Chen, Y. Zhou, K. Lei, L. Wang, W. Liu, H. Huang and T. Ma, Angew. Chem. Int. Ed., 2022, 61, e202200413.
20. D. Chen, W. Chen, Y. Wu, L. Wang, X. Wu, H. Xu and L. Chen, Angew. Chem. Int. Ed., 2023, 62, e202217479.
21. W. Zhao, P. Yan, B. Li, M. Bahri, L. Liu, X. Zhou, R. Clowes, N. D. Browning, Y. Wu, J. W. Ward and A. I. Cooper, J. Am. Chem. Soc., 2022, 144, 9902-9909.
22. J.-Y. Yue, L.-P. Song, Z.-X. Pan, P. Yang, Y. Ma, Q. Xu and B. Tang, ACS Catal., 2024, 14, 4728-4737.
23. X. Wang, Y. Jin, N. Li, H. Zhang, X. Liu, X. Yang, H. Pan, T. Wang, K. Wang, D. Qi and J. Jiang, Angew. Chem. Int. Ed., 2024, 63, e202401014.
24. M. Deng, L. Wang, Z. Wen, J. Chakraborty, J. Sun, G. Wang and P. Van Der Voort, Green Chem., 2024, 26, 3239-3248.
25. C. Shu, L. Wang, X. Yang, W. Xie, P. Xie, X. Wang, X. Yang, J. Rao, K. Wang, L. Chen, B. Tan and X. Wang, Nat. Commun., 2026, 17, 3046.
26. P. Zhang, H. Zeng, Q. Zhang, P. Wang, H. Che, C. Tang, J. Xu, J. Long, B. Liu and Y. Ao, Nat. Commun., 2026, 17, 3365.
27. Q. Liao, Z. Zhang, Z. Li, C. Shao, Q. Yan, M. Guo and D. Wang, ACS Appl. Energy Mater., 2026, 9, 4313-4321.
28. Y. Zhou, C. You, B. Hu, Y. Ma and C. Liu, J. Alloys Compd., 2026, 1056, 186640.
29. B. Lin, D.-H. Si, J.-J. Li, S.-Y. Gao, X. Yang and R. Cao, Adv. Mater, 2026, 38, e20022.
30. J. Chen, J. Zhou, N. Li, Y. Liu, X. Deng, F. Gou, Z. Yang, M. Zeng, M. Shao and Y. Guo, Chem. Sci., 2026, https://doi.org/10.1039/D5SC09083K.
31. L. Luo, S. Wang, L. Zhang, X. Xiao, B. Wu, M. Jaroniec and B. Jiang, Appl. Catal. B: Environ., 2024, 343, 123475.
32. W. Wang, Z. Shu and J. Zhou, Sep. Purif. Technol., 2025, 354, 129435.

33. B. Yan, Q. Ruan, S. Wang, L. Kong, P. Zhang, H. Wang and Z. Sun, Adv. Funct. Mater., 2024, 34, 2408895.
34. V. W. h. Lau, D. Klose, H. Kasap, F. Podjaski, M. C. Pignié, E. Reisner, G. Jeschke and B. V. Lotsch, Angew. Chem. Int. Ed., 2016, 56, 510-514.
35. J. Kröger, A. Jiménez-Solano, G. Savasci, P. Rovó, I. Moudrakovski, K. Küster, H. Schlomberg, H. A. Vignolo-González, V. Duppel, L. Grunenberg, C. B. Dayan, M. Sitti, F. Podjaski, C. Ochsenfeld and B. V. Lotsch, Adv. Energy Mater., 2021, 11, 2003016.
36. Y. Pan, J. Wang, S. Chen, W. Yang, C. Ding, A. Waseem and H.-L. Jiang, Chem. Sci., 2022, 13, 6696-6703.
37. P. M. Stanley, F. Sixt and J. Warnan, Adv. Mater., 2023, 35, 2207280.
38. S. Wu, P. M. Stanley, S. N. Deger, M. Z. Hussain, A. Jentys and J. Warnan, Angew. Chem. Int. Ed., 2024, 63, e202406385.
39. S. Yao, K. Heinzerling, S. A. J. Hillman, F. Podjaski, T. He, A. García-Baldoví, Y. Baghdadi, K. Dassouki, H. García, S. Eslava, N. Steunou, S. Gonzalez-Carrero, S. Navalón, G. Mouchaham, C. Serre and J. R. Durrant, Adv. Mater., 2026, 38, e17595.
40. M. Wang, G. Tan, B. Zhang, Y. Wang, Y. Bi, Q. Yang, Y. Liu, T. Liu, Z. Wang, H. Ren, L. Lv, A. Xia, L. Yin, Q. Yuan, W. Liu and Y. Liu, Appl. Catal. B: Environ., 2023, 321, 122052.
41. Y. Wang, Y.-T. Chan, T. Oshima, V. Duppel, S. Bette, K. Küster, A. Gouder, C. Scheurer and B. V. Lotsch, J. Am. Chem. Soc., 2024, 146, 25467-25476.